# Large-Area Mechanically-Exfoliated Two-Dimensional Materials on Arbitrary Substrates

*Satyam Sahu, Golam Haider, Alvaro Rodriguez, Jan Plšek, Martin Mergl, Martin Kalbáč, Otakar Frank, and Matěj Velický\**

**Atomically-thin crystals have been shown to be rich in fundamental phenomena and are promising for various applications. Mechanical exfoliation of (2D) materials from bulk crystals is particularly suited for fundamental studies due to the high quality of the resulting monolayer crystals. To date, several techniques have been developed to increase the exfoliation yield, however, they still suffer drawbacks. In this work, a novel method that exploits gold-assisted exfoliation to prepare large-area monolayers of various layered materials followed by their transfer to arbitrary substrates is introduced. X-ray photoelectron, Raman, and photoluminescence spectroscopies are employed to assess the quality of the prepared layers and their optical properties. Then, field-effect transistors and photodetectors are fabricated to demonstrate the suitability of this technique for large-area optoelectronic devices.**

## 1. Introduction

Since the discovery of graphene in 2004,[1] there has been a lot of interest in 2D materials because of their unique and tunable physical, chemical, and mechanical properties resulting from

S. Sahu, G. Haider, A. Rodriguez, J. Plšek, M. Mergl, M. Kalbáč, O. Frank, M. Velický
J. Heyrovský Institute of Physical Chemistry
Czech Academy of Sciences
Dolejškova 2155/3, 182 23 Prague 8, Czech Republic
E-mail: matej.velicky@jh-inst.cas.cz
S. Sahu
Department of Biophysics
Chemical and Macromolecular Physics
Faculty of Mathematics and Physics
Charles University
Ke Karlovu 3, 121 16 Prague 2, Czech Republic
A. Rodriguez
Materials Science Factory
Instituto de Ciencia de Materiales de Madrid
Consejo Superior de Investigaciones Científicas
Madrid 28049, Spain

their reduced dimensionality.[2–8] Due to the aforementioned properties and extreme sensitivity to the environment, monolayers of layered materials can be used in wide ranging applications such as ultra-high performance optoelectronics, sensors, flexible electronics, energy conversion and storage, biomedicine, and defense.[9–15]

At a laboratory level, preparation of monolayers (1L) of 2D materials is straightforward as small individual flakes on the order of tens of μm in lateral size usually suffice. However, the utility of 2D materials at an industrial level is still limited by the conflicting relation between the size and quality of 1L flakes. Numerous research groups have focused on preparation of large-area 2D materials using the most common methods including mechanical exfoliation, chemical vapor deposition (CVD), liquid-phase exfoliation, etc., each with specific pros and cons. For example, directly mechanically exfoliated flakes are considered of the highest quality but achieving 1L flakes larger than few tens of microns is a challenge.[7,16] On the contrary, CVD can produce 1L flakes a few cm in lateral size, but controlling the parameters and conditions is tedious[17] and the high temperature[18] (≈800 °C) needed for the growth of high-quality layers increases the costs and is often incompatible with direct device fabrication. Moreover, samples prepared using CVD or related methods contain vacancies and grain boundaries, which modify the properties of the resulting material.[19] The grain sizes for samples prepared using these methods lie in few μm range,[20] which undermines their (opto)electronic applications because of the increased carrier scattering at grain boundaries. Liquid-phase exfoliation is a viable route for scalable production of 1L flakes, whose quality, however, is poor. All these disadvantages combined limit the applications of 2D materials in both research and industry.

Recently, several research groups have reported on mechanical exfoliation of large-area monolayers on gold substrates.[21–25] This method relies on the fact that clean Au interacts strongly with the closest layer of the bulk layered materials, particularly chalcogenides such as $MoS_2$, since the van der Waals (vdW) interaction between Au and the closest 2D layer is larger than the vdW interaction between the closest 2D layer and the rest of the layered material.[23] The effect of this interaction on the electronic band structure of the 2D material can be observed in the Raman and photoluminescence (PL) spectra, X-ray photoelectron

**ADVANCED
SCIENCE NEWS**

www.advancedsciencenews.com

**ADVANCED
MATERIALS
TECHNOLOGIES**

www.advmattechnol.de

spectra (XPS), and scanning tunneling microscopy/spectroscopy. We previously observed a sizeable shift in the Raman vibration frequencies along with the splitting in the $A_1$ mode of 1L $MoS_2$ on Au and predicted a bandgap closure for this system, which does not only result in quenching of PL, but also limits their utility for (opto)electronic applications.[23,26] Thus, a method of transferring the large-area monolayers from Au to another, arbitrary substrate in order to eliminate the undesirable effects of Au, is of utmost importance.

Several works demonstrated the transfer of large exfoliated monolayers from Au to different substrates without damaging the optoelectronic properties of monolayers.[22,24,27–29] Most of those studies employed a spin-coated polymer or used thermal release tape as a supporting layer to transfer the monolayers to the target substrate. These protocols were exploited to build patterned heterostructures as well as optoelectronic devices.[30–33] However, none of the mentioned protocols achieved a precise control of the flake positioning, which is essential for the design and fabrication of large area optoelectronic devices.

In this work, we present a facile and time-efficient method capable of preparing large 2D monolayers on arbitrary substrates that allows the exfoliation of common TMDCs ($MoS_2$, $MoSe_2$, $WS_2$, $WSe_2$, etc.) as well as less-studied materials such as $PtSe_2$, which are very difficult to exfoliate on $SiO_2/Si$ along, especially with sample positioning control. It is based on the combination of the chemically etched, Au-assisted exfoliation and deterministic transfer method using a viscoelastic stamp. We characterize the prepared layers using XPS, Raman, and PL spectroscopies. As a proof-of-concept of the utility of our method, we also prepare a large-area vdW heterojunction of two monolayers of different semiconducting 2D materials. Finally, we fabricated a phototransistor using the transferred 1L $MoS_2$. The optoelectronic performance of the photo-device shows behavior consistent with the reported devices based on 2D materials exfoliated directly onto dielectric substrates. We believe that our study constitutes a major step toward mm- and cm-scale devices based on large-area exfoliation of high-quality 2D materials.

## 2. Results and Discussion

The schematic of our exfoliation and transfer process is shown in **Figure 1**a. We first cleaned the $SiO_2/Si$ substrates by sonication in acetone and isopropanol (5 min each) and blow-dried them with nitrogen gas (i). We then deposited thin layers of Cr/Au (4 nm/10 nm) on $SiO_2/Si$ substrates using magnetron sputtering (ii). All 2D materials were then immediately exfoliated from bulk crystals directly onto the Au-coated substrates using the "scotch-tape" method reported elsewhere (iii, iv).[34] The sizes of the 1L flakes obtained on the Au-coated substrate reached 25 $mm^2$ (Figure S1, Supporting Information), limited only by the size of the bulk layered crystals.

For the transfer of 1L flakes, we have adopted a different approach to those reported in the literature to date. Instead of spin-coating a polymer layer on top of the 2D material, we utilize ready-to-use polydimethylsiloxane (PDMS) stamps (Gel Pak 4 by GelPak Inc.). First, we stamp the PDMS on the Au-coated $SiO_2/Si$ substrate with the exfoliated monolayers (v). Next, the PDMS/1L/substrate stack is placed in a $KI/I_2$ gold etchant solution (Thermo Fisher Scientific Inc.). $KI/I_2$ solution etches away

the Au and causes the PDMS/1L stack to lift off of the substrate and float on the liquid surface (vi). The whole transfer process following the exfoliation on Au takes less than 30 min, which is significantly faster than in earlier reports where the samples were kept in the solution for 10 h.[24] The PDMS/1L stack is then rinsed with 0.1 M KCl solution (two times) to wash the remaining Au from the surface of the 2D material, followed by rinsing with distilled water (three times) to remove the KCl residues (vii). Next, the PDMS/1L stack is scooped using a glass slide, flipped on a support substrate (thick PDMS) (viii), and blow-dried with $N_2$. The sample is now ready for the final transfer step to a target substrate. We then align the PDMS/1L stack with the target substrate, bring them in contact with the help of a micromechanical transfer stage (ix), and heat for 15 s at 70 °C. Finally, the PDMS film is peeled off leaving the large-area flakes on the arbitrary target substrate (x). This protocol allows to transfer very large monolayers with the help of PDMS rather than using direct exfoliation on PDMS. Direct exfoliation on PDMS is not only very tedious due to the need of identifying the 1L flakes in the optical microscope but it usually provides smaller flakes of only tens of μms in lateral size. Once the 2D flakes are placed on PDMS, they can subsequently be transferred to any substrate by using common transfer setups.

Optical microscopy was used to examine the dimensions and uniformity of the transferred 1L flakes. Figure 1b–g shows the optical images of 2D materials transferred onto 300 nm $SiO_2/Si$ substrates, including transition metal dichalcogenides and graphene. Besides $SiO_2/Si$, we used quartz, borosilicate glass, and flexible plastics (polyethylene terephthalate) as target substrates for the transfer of 1L $MoS_2$ flakes (Figure S2, Supporting Information). The number of layers was determined from the optical contrast of the transferred flakes.

High transfer yield and preservation of crystalline quality are the key parameters of the transfer process efficiency. Therefore, we measured the 1L flake areal coverage before and after the transfer, yielding ≈ 90% transfer efficiency in the case of 1L $MoS_2$ on $SiO_2/Si$ (Figure S3, Supporting Information). We employed the XPS analysis of the transferred 1L $MoS_2$ to determine the chemical composition and impurity content (Au, K, I, etc.). The atomic ratio of 1.6 between Mo and S confirms the presence of commonly occurring sulfur vacancies, although the exact ratio is unreliable due to the low absolute concentrations. The survey spectrum (Figure S4, Supporting Information) reveals the absence of both K and I. The Au concentration is also near or below the XPS detection limit (Figure S4, Supporting Information). **Figure 2**a shows the high-resolution core-level XPS spectra of the Mo 3d and S 2s orbitals. The spectrum in Figure 2a was fitted with two Gaussian–Lorentzian doublets with well separated (Δ = 3.15 eV) spin-orbit components of Mo 3d (229.7/232.9 eV for $Mo^{4+}$ and 233.6/236.8 eV for $Mo^{6+}$) and one Gaussian–Lorentzian for S 2s (226.5 eV). The low intensity peak at 233.6 eV belongs to the oxidized Mo species. The S 2p spectrum in Figure 2b was fitted as a doublet ($2p_{3/2}$ and $2p_{1/2}$) yielding binding energies of 162.6 and 163.7 eV, respectively. The peak positions in the Mo 3d spectrum were also compared with those of the 1L $MoS_2$ exfoliated on Au and bulk $MoS_2$ (Figure S5, Supporting Information). The high-energy Mo 3d component for $MoS_2$/Au sample was shifted by ≈0.4 eV and it can be assigned to the $MoS_2$ layer closest to the Au substrate.[35] Similar shape of the Mo and S spectra for the
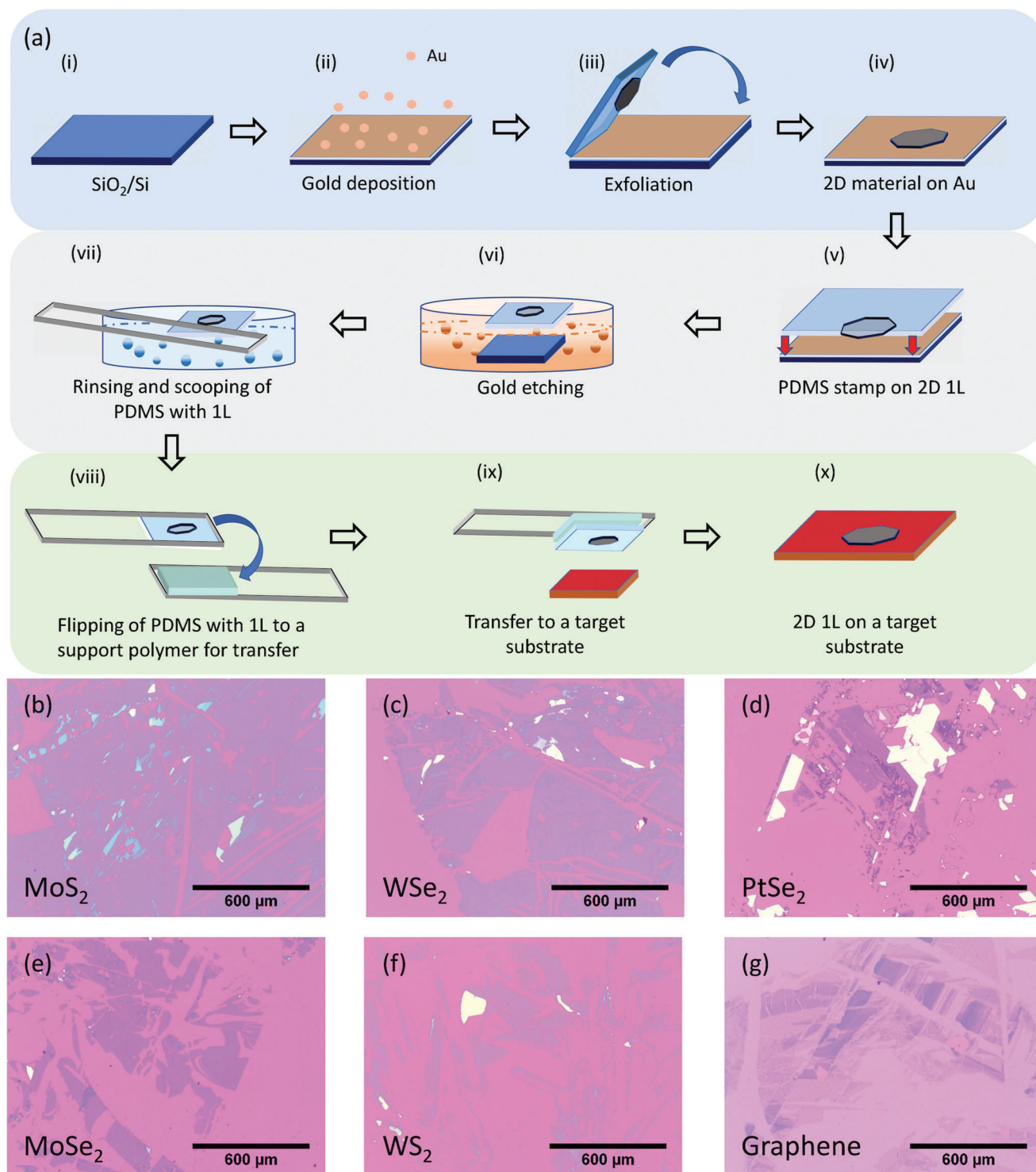
**Figure 1.** 2D material preparation method combining the gold-assisted exfoliation and deterministic transfer using PDMS. a) Schematic of the exfoliation/transfer process: (i) cleaned $SiO_2$/Si substrate, (ii) deposition of Au, (iii) tape exfoliation of bulk layered crystal on Au-coated $SiO_2$/Si substrate, (iv) 1L flake on the Au-coated substrate, (v) PDMS stamp placed on 1L/Au substrate, (vi) etching of gold, (vii) PDMS/1L stack was cleaned using KCl and distilled water and scooped using a glass slide, (viii) PDMS/1L was flipped on a thick PDMS support, (ix) PDMS/1L stack placed on the target substrate, (x) 1L on the target substrate. b–g) Optical microscopy images of 1L flakes transferred onto an $SiO_2$/Si substrate. All scale bars correspond to 600 µm.
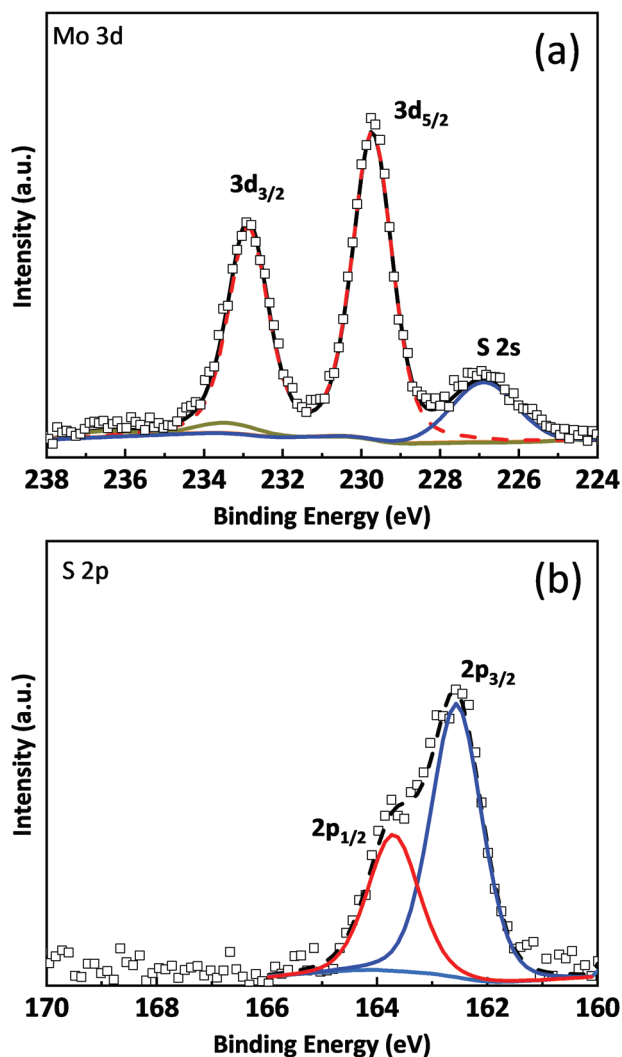
**ADVANCED
SCIENCE NEWS**

www.advancedsciencenews.com

**ADVANCED
MATERIALS
TECHNOLOGIES**

www.advmattechnol.de

**Figure 2.** High-resolution XPS of 1L MoS$_2$ transferred to SiO$_2$/Si. a) Mo 3d and b) S 2p spectral regions of monolayer MoS$_2$ prepared by gold-assisted exfoliation and transfer to SiO$_2$/Si. The binding energies were obtained from Gaussian–Lorentzian fits of the baseline-subtracted Mo 3d and S 2p spectra. The black lines show the sum of all the convoluted peaks and the empty boxes show the raw data in both (a) and (b).

transferred and directly exfoliated samples therefore indicates that the transferred samples maintain structural and chemical integrity after transfer.

To further compare the properties of the directly exfoliated samples with samples prepared using our method, we performed atomic force microscopy (AFM) and Raman and PL spectroscopy measurements. AFM provides an independent measurement of the surface morphology of the monolayers. On the other hand, Raman and PL spectroscopies inform one about the mechanical strain, charge carrier density, and band gap. **Figure 3**a,b shows the optical and AFM image of the transferred 1L MoS$_2$ flake of a selected area of the sample.

It is evident from the topography images shown in Figure S6, Supporting Information that the surfaces of samples transferred using our method have similar morphologies as those of directly

exfoliated samples. Raman spectra in Figure 3c show the two main vibrational modes, E$'$ (in-plane) and A$_1'$ (out-of-plane), of MoS$_2$.[35,36] Crucially, we do not see any significant shifts in the positions of the Raman modes between the transferred MoS$_2$ and MoS$_2$ directly exfoliated on SiO$_2$/Si. This is in contrast to MoS$_2$ on Au, where large shifts in the peak positions, splitting of A$_1'$, and emergence of symmetry/geometry forbidden modes are observed.[35,37] The similarity between the transferred and directly exfoliated samples confirms that MoS$_2$ is not chemically modified during exfoliation on Au and does not retain any residual strain after transferring from Au to SiO$_2$/Si. The PL spectrum of the transferred MoS$_2$, composed of the neutral (A) and charged (A$^-$) excitons reveals a slight energy blueshift and a change in the spectral shape in comparison to the directly exfoliated MoS$_2$, as shown in Figure 3d. These differences could be attributed to minor variations in charge doping, corroborated by the slight shift of the A$_1'$ Raman mode.[38] Similar effects were observed for other TMDCs as well (Figures S9 and S15, Supporting Information). We also exfoliated and transferred graphene monolayers using our method. While the Au-assisted exfoliation was reported to be less effective for graphene due to the small adhesive energy between graphene and Au,[24] we were able to exfoliate relatively large graphene monolayers by heating the substrate to 80 °C for 15 s.

Figure 3e–g shows the optical and AFM images of monolayer graphene transferred on SiO$_2$/Si after exfoliation on Au, and the Raman spectra of the transferred and directly exfoliated graphene on SiO$_2$/Si, respectively. Since the Raman spectrum of graphene is more sensitive to defects than that of MoS$_2$, we proceed to analyze the former in greater detail. We observe both the main G and 2D modes of graphene; however, the D mode activated by defects in the ≈1340–1350 cm$^{-1}$ range is not present (Figure S7, Supporting Information),[39] which confirms the absence of a significant amount of disorder in our samples. For the case of graphene on Au, we observe a clear shift as a result of the charge transfer and/or strain. The average (20 spectra) Raman frequencies of the G and 2D modes for monolayer graphene prepared using our method (Au-assisted exfoliation followed by transfer) are 1581.2 ± 0.5 and 2672.3 ± 1.9 cm$^{-1}$, respectively. The corresponding averages for the directly exfoliated samples are 1580.7 ± 1.6 and 2670.9 ± 3.3 cm$^{-1}$, respectively. The correlation analysis of the G and 2D Raman positions (Figure S8, Supporting Information) reveals that the individual data points mostly differ in strain, as do the average G and 2D position values. Quantitatively, the sample transferred by our method shows a minor compression (by approximately −0.014%) relative to the directly exfoliated graphene,[40] and a slightly lower carrier density (by ≈1 × 10$^{11}$ cm$^{-2}$).[41] Furthermore, we observe a narrowing of the 2D linewidth along with an increase in I$_{2D}$/I$_G$ ratio to 3.6 for the samples prepared using our method. The I$_{2D}$ depends on several factors such as electron–phonon coupling, electron–defect scattering, electron–electron scattering rate, etc., and its sensitivity to changes in carrier density is much higher at low doping levels (between the charge neutrality point and Fermi energy corresponding to the phonon anomaly).[41] For that reason, I$_{2D}$ can vary significantly from sample to sample as discussed explicitly by Froehlicher et al.[42] and the I$_{2D}$/I$_G$ ratio is therefore not an ideal parameter to fully explain the strain and doping effects. Nevertheless, its increase also suggests a partial de-doping
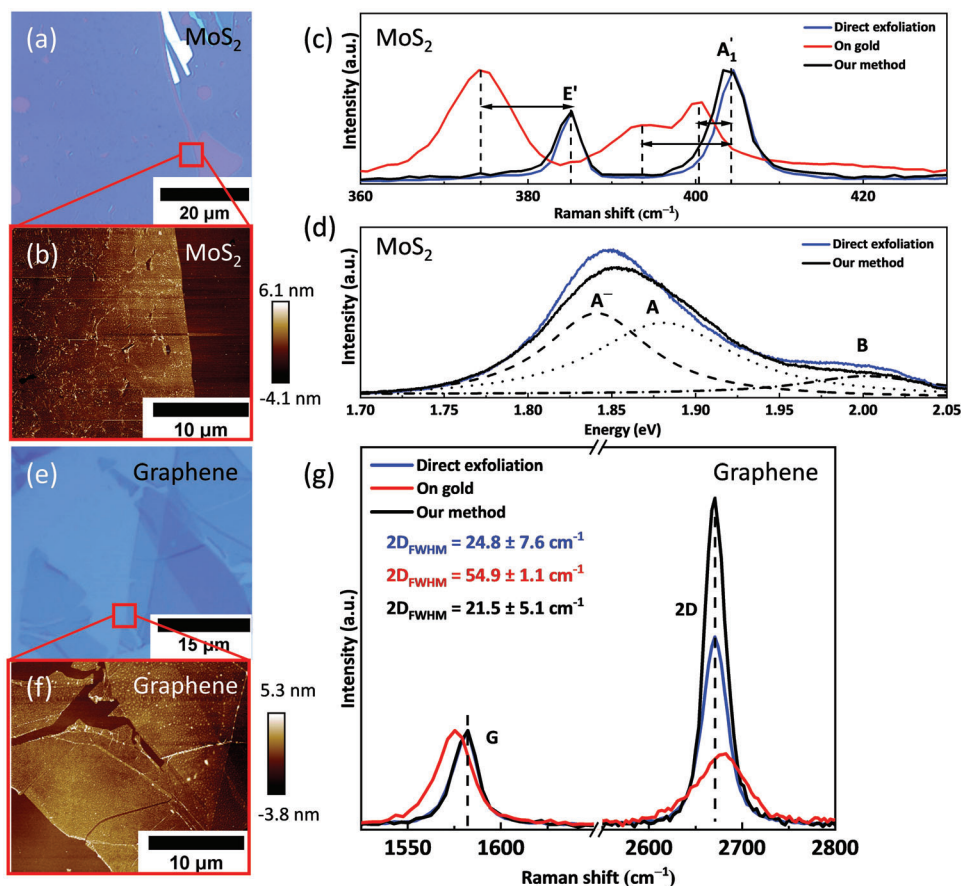
**ADVANCED
SCIENCE NEWS**

www.advancedsciencenews.com

**ADVANCED
MATERIALS
TECHNOLOGIES**

www.advmattechnol.de

**Figure 3.** Raman spectroscopy, PL spectroscopy, and AFM of $MoS_2$ and graphene monolayers prepared using different methods. a) Optical image of $MoS_2$ prepared by gold-assisted exfoliation followed by transfer to $SiO_2/Si$ using PDMS (our method). b) AFM image of a selected area of $MoS_2$ in (a). c) Raman spectra of $MoS_2$ directly exfoliated on $SiO_2/Si$ (blue), exfoliated on gold (red), and transferred to $SiO_2/Si$ using our method (black). d) PL spectra of $MoS_2$ directly exfoliated (blue) and transferred using our method (black). e) Optical image of graphene transferred to $SiO_2/Si$ using our method. f) AFM image of a selected area of graphene in (e). g) Raman spectra of graphene directly exfoliated (blue), exfoliated on gold (red), and transferred to $SiO_2/Si$ using our method (black) monolayer graphene. Laser excitation of 532 nm was used throughout.

(charge carrier density decrease) of graphene toward its native, undoped state, in contrast to its p-doped state when directly exfoliated on $SiO_2/Si$.[41,43] The decrease in the 2D band linewidth also evidences larger strain and/or doping homogeneity within the laser spot,[44] in line with the smaller spread of the G and 2D mode frequencies shown in Figure S8, Supporting Information.

Since our method relies on the transfer of 1L flakes using a PDMS stamp, we can use it to construct vdW homo- or hetero-structures. **Figure 4** shows characterization of a typical $MoSe_2/MoS_2$ hetero-bilayer assembled using our method ($MoSe_2$ on top of $MoS_2$). In the left panel, Raman spectra corresponding to $MoS_2$, $MoSe_2/MoS_2$, and $MoSe_2$ are shown. The Raman mode frequencies for the $MoSe_2/MoS_2$ heterostructure are matching well those of the individual materials, indicating a weak interaction between the two monolayers. In the right panel, PL spectra of the same samples are shown. The A exciton of $MoS_2$, composed of the neutral exciton A and charged trion $A^-$, is located at 1.88 eV and the B exciton is at 2.05 eV. In the case of $MoSe_2$, the excitonic A peak at 1.57 eV is symmetric and the B type exciton is also visible at around 1.75 eV. Two remarks should be made regarding the PL spectra of the $MoSe_2/MoS_2$ heterostructure. First,

the $MoS_2$ PL peak position redshifts and second, its intensity decreases, in comparison to pristine $MoS_2$. These observations can most likely be attributed to the interlayer charge transfer and/or strain in the top layer localized in bubbles and blisters.[45,46]

As mentioned earlier, although the large-sized flakes can easily be exfoliated on Au, metallic substrates are not suitable for electrical and optoelectronic studies and applications. For such purposes, an additional transfer step to a dielectric substrate is needed. In this section, we demonstrate the utility of our method to prepare a device, which can be utilized in optoelectronics. To that end, we fabricated a Hall bar device using $MoS_2$ transferred to $SiO_2/Si$ and measured its mobility (see Section S16, Supporting Information for details). The calculated mobility was 0.86 cm$^2$ V$^{-1}$ s$^{-1}$, which is lower in comparison to that of the typical field-effect transistor (FET) devices prepared from $MoS_2$ transferred on $SiO_2/Si$.[24,47] We then extended our approach to an array of FETs (Figures S10 and S11, Supporting Information), which indicates the utility of our transfer approach for the integrated circuit design and its potential for the field of complex electronics.

We further used our method to design a phototransistor and demonstrate its utility toward the integration within state-of-
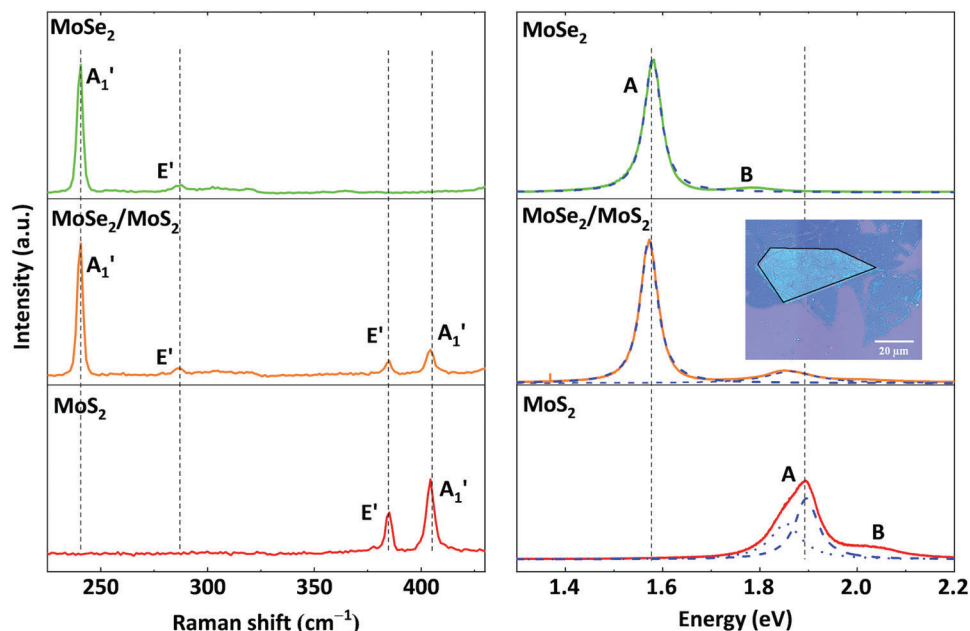
**ADVANCED**
**SCIENCE NEWS**
www.advancedsciencenews.com

**ADVANCED
MATERIALS
TECHNOLOGIES**
www.advmattechnol.de

**Figure 4.** Raman and PL spectroscopy of heterostructures fabricated via sequential transfer of large monolayers. (Left panel) Raman spectra of $MoSe_2$ (green), $MoSe_2/MoS_2$ heterostructure (orange), and $MoS_2$ (red). (Right panel) PL spectra of $MoSe_2$ (green), $MoSe_2/MoS_2$ heterostructure (orange), and $MoS_2$ (red) taken at room temperature using 532 nm excitation wavelength at 50 µW of power. Blue dashed (dotted) lines in PL spectra show the Lorentzian fitting of the neutral (charged) excitons. Inset: optical image of the $MoSe_2/MoS_2$ heterostructure, scale bar: 20 µm.

the-art optoelectronic circuits. In **Figure 5**, we show a proof-of-concept photodetector device based on 1L $MoS_2$. Schematic representation and optical images of the device are shown in Figures 5a–c. To investigate the device performance, we first recorded the drain-source current-voltage ($I_{ds}-V_{ds}$) output characteristics in the dark and under illumination, using a focused laser beam ($\lambda = 514.5$ nm) of different illumination power densities in the range 2.5 to 63.6 µW cm$^{-2}$, as shown in Figure 5d. The linearity and symmetry of the $I_{ds}-V_{ds}$ curves for small $V_{ds}$ indicate an ohmic contact, and show an increase of $I_{ds}$ by several orders of magnitude upon illumination. The photocurrent ($I_{ph} = I_{illuminated}-I_{dark}$, where $I_{illuminated}$ and $I_{dark}$ are the drain–source currents under laser illumination and in the dark, respectively) also increases with $V_{ds}$ as a result of increase in carrier density. All the other measurements were performed under low $V_{ds}$ to avoid heating of the sample. The temporal photoresponse of the FET under different incident laser power densities at $V_{ds} = 1$ V and gate voltage ($V_g$) = 0 V is shown in Figure 5e. Upon turning the laser on, $I_{ds}$ increases promptly and saturates within a few seconds. When the laser is turned off, $I_{ds}$ decreases toward the dark current background level, which is a photovoltaic behavior expected for a semiconducting device. The dependence of photocurrent on illumination density shown in Figure 5f was fitted using a power law ($I_{ph} \approx P^c$, where $P$ is the illumination density and $c = 0.84$ is the fitted exponential parameter). At low illumination power densities (below 22.9 µW/cm$^2$), the photocurrent shows a near-linear dependence on the illumination density, which is a signature of low defect density in $MoS_2$. In contrast, it has been shown that defects induces a nonlinear dependence of the photocurrent with the excitation power density, as the trap states fill up with photo-carriers.[48,49] Similar behavior was observed for the power-dependent PL of monolayer $MoS_2$

prepared using our method (Figure S12, Supporting Information). The photocurrent ON/OFF ratio ($I_{illuminated}/I_{dark}$) follows a similar trend as $I_{ph}$ achieving the maximum of 72 at 63.6 µW cm$^{-2}$. The photodetector response had a typical rise time of 40 ms and decay time of 60 ms under 2.5 µW cm$^{-2}$ illumination power density (Figure S13, Supporting Information), which is comparable to earlier reports.[9]

One of the most important figures of merit for a photodetector is its responsivity ($R = I_{ph}/P$, where $P$ is the power used by the device). For our device, the responsivity was found to be ≈47 A/W for $V_{ds} = 1$ V and 1.27 µW cm$^{-2}$, and ≈2200 A W$^{-1}$ for 10 V and 63.6 µW cm$^{-2}$. The observed responsivity values are comparable with the reported values of typical $MoS_2$-based devices produced by direct exfoliation method for similar $V_{ds}$ and power density.[9] Figure 5g shows the variation in detectivity, $D = R\sqrt{A/(2eI_{dark})}$, where $A$ is the device area, and photocurrent gain, $\eta = R(hc/e\lambda)$, where $\lambda$ is the wavelength of the incident light, with illumination power density. The responsivity decreases with an increase in illumination power as a result of unbalanced electron–hole pair generation. This happens by virtue of saturable absorption and defect saturation at higher illumination intensities. Moreover, due to the nonlinear I–V characteristics of the FET, the photocurrent increases superlinearly with the increase of source–drain voltage, giving rise to increased responsivity.[9] We are aware of the fact that the photocurrent in such devices is position-dependent.[50,51] In order to reduce the power density, we intentionally broadened the excitation spot size, which extended beyond the device area. Hence the obtained photocurrent in low-intensity regime may have the contribution from the flake outside of the device active area, which we have ignored for the proof-of-concept demonstration. The values obtained for all figure of merit parameters for the device prepared using our method were comparable to the
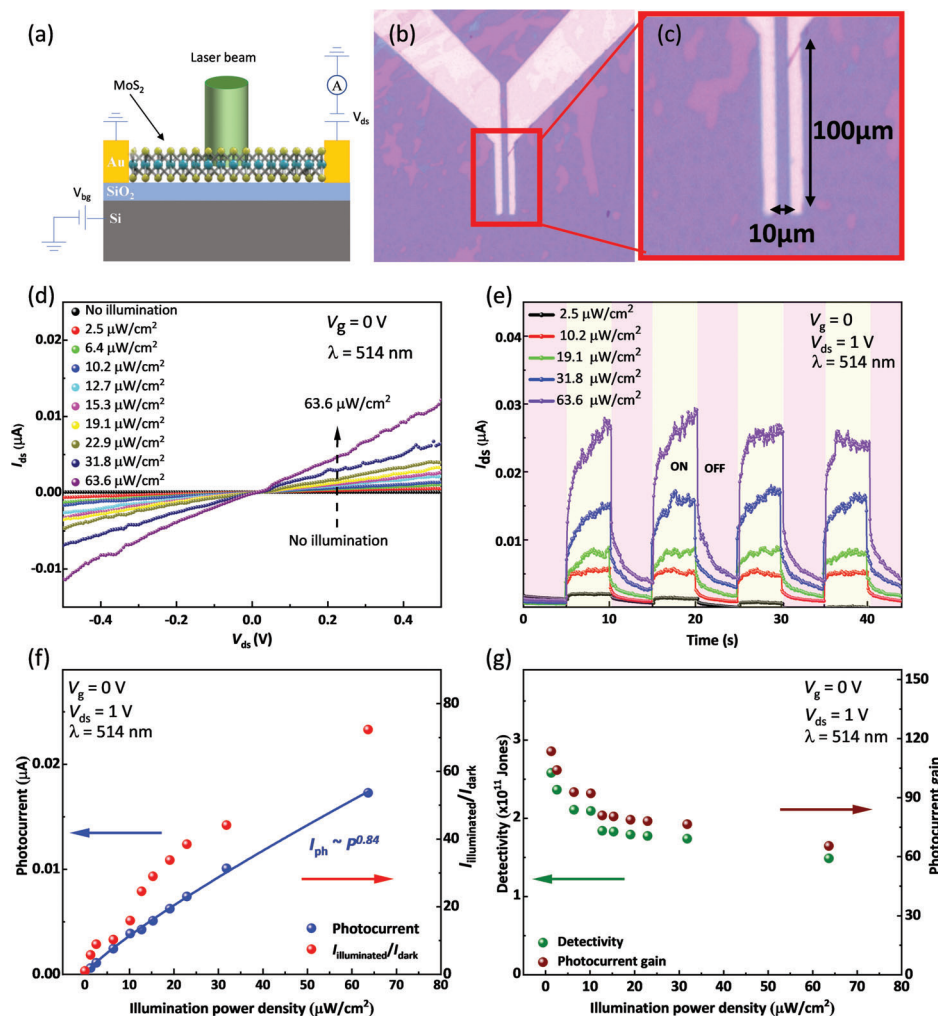
**ADVANCED
SCIENCE NEWS**

www.advancedsciencenews.com

**ADVANCED
MATERIALS
TECHNOLOGIES**

www.advmattechnol.de

**Figure 5.** Phototransistor based on the MoS$_2$ monolayer on SiO$_2$/Si using the Au-assisted exfoliation followed by transfer. a) Schematic of the photodetector device. b,c) Optical images of the photodetector device. The active area of the device was 1000 μm$^2$. d) Drain–source ($I_{ds}$–$V_{ds}$) characteristic of the device in the dark and under different illumination power densities. e) Temporal photoresponse of the device to a laser pulse of 514 nm under different illumination power densities at $V_{ds} = 1$ V and $V_g = 0$ V. f) Variation in photocurrent (left) and ON/OFF ratio (right) with illumination power density. g) Detectivity (left) and photocurrent gain (right) at different illumination power densities.

values reported in the literature.[9,52] Even after 5 months, the device showed outstanding performance and the values of photocurrent were about 80% of the initial current (Figure S14, Supporting Information). These values combined with XPS and Raman data prove that the transferred MoS$_2$ monolayers preserve its high crystalline quality.

## 3. Conclusions

Our results demonstrate the advantages of the Au-assisted exfoliation and subsequent transfer to an arbitrary substrate over existing methods. This method is suitable for the preparation of 2D materials, which cannot be exfoliated to large-area monolayers using mechanical exfoliation due to interlayer interactions stronger than those between the substrate and the adjacent 2D layer but can be readily exfoliated on Au (e.g., PtSe$_2$). Hence, our method makes such materials available for fundamental studies and applications. While significant progress has been made in

developing efficient ways of transferring 2D materials to other substrates, our methods provides the fastest route to date thanks to the avoidance of the spincoating step, absence of which significantly speeds up the etching rate of Au (less than 30 min). Characterization of the transferred, large-area monolayers confirms that the 2D flakes are of high quality. We apply our method to design a large-area 2D heterostructure and study its optical properties. Finally, we show that our method is suitable for fabrication of optoelectronic devices requiring large-area samples of high-quality. We demonstrate this utility by fabricating FET and photodetector devices with characteristics of high-quality mechanically exfoliated monolayers.

## 4. Experimental Section

*Mechanical Exfoliation on Gold Substrates*: The metal layer deposition was completed in a sputtering system Quoram Q300T D (Quorum Inc., UK). An adhesive layer of Cr was deposited on an SiO$_2$/Si substrate,

after that a layer of Au was deposited. After depositing the metal layer, the 2D flakes were directly exfoliated from a bulk crystal (Manchester Nanomaterials Ltd., 2D Semiconductors Ltd., and Hq graphene Ltd.) using a low-adhesion tape (Nitto Denko Corp.). The yield of monolayers was usually only limited by the size of the parent crystal, but the morphology and history of the Au surface also played a role.[23,35] It was observed that for a thinner Au film, the area covered by monolayer was larger, while for thicker Au films (>15 nm Au), the flake-covered area was relatively smaller. In this case, the optimum thickness of Au was 10 nm and Cr was 4 nm. The yield of large area monolayers also depend on the time for which the Au-coated substrate was kept under the ambient conditions.[23]

*Preparation of Heterostructures by Stacking Of Large Monolayers*:   To prepare the heterostructure, first 1L $MoS_2$ was exfoliated and transferred onto the $SiO_2$/Si substrate using the method described in Figure 1a. Then, 1L $MoSe_2$ was separately exfoliated and transferred onto a PDMS stamp, up to the step (viii) in Figure 1a. Then, 1L $MoSe_2$ was transferred on top of 1L $MoS_2$ using a commercial transfer stage. No special alignment was needed in this step as the twist angle between these two layers was not specified. Additional annealing at 200 °C was done to improve the contact between the two layers.

*Fabrication of Monolayer $MoS_2$ Phototransistor and Hall Bar Devices*: For the fabrication of the devices, first, monolayer $MoS_2$ was prepared on PDMS using the method. Then, the electrodes were patterned on cleaned $SiO_2$/Si (300 nm) substrates with a direct-write lithography technique, and subsequently, 10 nm Cr and 40 nm Au was evaporated. This was followed by a direct transfer of $MoS_2$ monolayer from PDMS to $SiO_2$/Si substrate with electrodes. To ensure proper contact between the electrodes and monolayer $MoS_2$, the samples were annealed at 200 °C in a quartz tube under argon atmosphere for 2 h.

*X-Ray Photoelectron Spectroscopy*:   The XPS measurements were performed in a VG ESCA3 MkII electron spectrometer with a base pressure better than $10^{-9}$ mbar. Al $K_\alpha$ radiation was used for the excitation of the electrons. The electrons were energy-analyzed using a hemispherical analyzer operating at constant pass energy of 20 eV. The spectra were calibrated by setting the main feature of Si 2p region to the binding energy of 103.5 eV. The high-resolution spectra of Mo 3d, S 2p, Si 2p, Au 4f, C 1s, and O 1s photoelectrons were measured. The surface atomic content was determined assuming a homogenous distribution of atoms and Scofield photoionization cross-section.

*Optical and AFM Characterization*:   Optical microscopy images were taken using an Olympus optical microscope with an Infinity 1-2 CCD camera and Infinity Capture software (Lumenera Corp). The transfer efficiency was calculated using a constant sampling area method. Identical regions of 25 $mm^2$ were chosen and the areas covered by 1L flakes before and after transfer were estimated using the Fiji/ImageJ software. The transfer efficiency was then calculated as $A_{after}/A_{before} \times 100\%$, where $A_{before}$ and $A_{after}$ are the 1L flake areas before and after transfer, respectively. Raman and PL measurements were performed on a commercial WITEC Alpha 300R spectrometer using a 532 nm diode laser at illumination powers of 500 or 50 $\mu W$ focused through a 100× MPlan N objective with ≈1 $\mu m^2$ spot size. AFM topography measurements were performed in a PeakForce tapping mode using a Bruker Icon instrument.

*Electrical Characterization*:   Electrical and optoelectronic measurements were performed using an in-house probe station equipped with a semiconductor parameter analyzer Keithley 2612B (Tektronix, Inc., USA). For optoelectronic measurements, $\lambda = 514.5$ nm line of an Ar–Kr laser were used and the illumination intensities were controlled using a variable neutral density filter. A microscope objective and a micromechanical stage were used to align the device to the center of the laser beam and an optical diffuser was used to broaden the laser beam area (0.78 $cm^2$) to uniformly illuminate the sample resulting in an estimated maximum illumination power density of 63.6 $\mu W$ $cm^{-2}$. Origin Pro 2019 Academic Edition was used for data analysis and graph plotting.

## Supporting Information

Supporting Information is available from the Wiley Online Library or from the author.

## Conflict of Interest

The authors declare no conflict of interest.

## Data Availability Statement

The data that support the findings of this study are openly available in the HeyRACK repository at https://doi.org/10.48700/datst.avcx3-w3h61.

[1] K. S. Novoselov, A. K. Geim, S. V. Morozov, D. Jiang, Y. Zhang, S. V. Dubonos, I. V. Grigorieva, A. A. Firsov, *Science* **2004**, *306*, 666.

[2] X. Yin, C. S. Tang, Y. Zheng, J. Gao, J. Wu, H. Zhang, M. Chhowalla, W. Chen, A. T. Wee, *Chem. Soc. Rev.* **2021**, *50*, 10087.

[3] K. Kośmider, J. W. González, J. Fernández-Rossier, *Phys. Rev. B* **2013**, *88*, 245436.

[4] P. R. Mol, P. K. Barman, P. V. Sarma, A. S. Kumar, S. Sahu, M. M. Shaijumon, R. N. Kini, *Nanoscale Adv.* **2021**, *3*, 5676.

[5] A. Castellanos-Gomez, M. Poot, G. Steele, H. van der Zant, *Adv. Mater.* **2012**, *24*, 772.

[6] S. Bertolazzi, J. Brivio, A. Kis, *ACS Nano* **2011**, *5*, 9703.

[7] M. Velický, M. A. Bissett, C. R. Woods, P. S. Toth, T. Georgiou, I. A. Kinloch, K. S. Novoselov, R. A. Dryfe, *Nano Lett.* **2016**, *16*, 2023.

[8] M. Velický, P. S. Toth, *Appl. Mater. Today* **2017**, *8*, 68.

[9] O. Lopez-Sanchez, D. Lembke, M. Kayci, A. Radenovic, A. Kis, *Nat. Nanotechnol.* **2013**, *8*, 497.

[10] M. Pumera, A. H. Loo, *Trends Anal. Chem.* **2014**, *61*, 49.

[11] X. Hu, W. Zhang, X. Liu, Y. Mei, Y. Huang, *Chem. Soc. Rev.* **2015**, *44*, 2376.

[12] D. Akinwande, N. Petrone, J. Hone, *Nat. Commun.* **2014**, *5*, 5678.

[13] D. Chimene, D. L. Alge, A. K. Gaharwar, *Adv. Mater.* **2015**, *27*, 7261.

[14] H. K. Adigilli, A. Pandey, J. Joardar, in *Handbook of Advanced Ceramics and Composites: Defense, Security, Aerospace and Energy Applications* (Eds: Y. Mahajan, J. Roy), Springer, Cham **2020**, pp. 75–120.

[15] P. Kaushik, F. J. Sonia, G. Haider, M. K. Thakur, V. Valeš, J. Kong, M. Kalbáč, *Adv. Mater. Interfaces* **2022**, *9*, 2200478.

[16] K. S. Novoselov, D. Jiang, F. Schedin, T. Booth, V. Khotkevich, S. Morozov, A. K. Geim, *Proc. Natl. Acad. Sci. U. S. A.* **2005**, *102*, 10451.

[17] L. Banszerus, M. Schmitz, S. Engels, J. Dauber, M. Oellers, F. Haupt, K. Watanabe, T. Taniguchi, B. Beschoten, C. Stampfer, *Sci. Adv.* **2015**, *1*, e1500222.

[18] Z. Cai, B. Liu, X. Zou, H.-M. Cheng, *Chem. Rev.* **2018**, *118*, 6091.

[19] J. Hong, Z. Hu, M. Probert, K. Li, D. Lv, X. Yang, L. Gu, N. Mao, Q. Feng, L. Xie, J. Zhang, D. Wu, Z. Zhang, C. Jin, W. Ji, X. Zhang, J. Yuan, Z. Zhang, *Nat. Commun.* **2015**, *6*, 6293.

[20] C. Lan, D. Li, Z. Zhou, S. Yip, H. Zhang, L. Shu, R. Wei, R. Dong, J. C. Ho, *Small Methods* **2019**, *3*, 1800245.

[21] G. Z. Magda, J. Pető, G. Dobrik, C. Hwang, L. P. Biró, L. Tapasztó, *Sci. Rep.* **2015**, *5*, 14714.

[22] S. B. Desai, S. R. Madhvapathy, M. Amani, D. Kiriya, M. Hettick, M. Tosun, Y. Zhou, M. Dubey, J. W. Ager III, D. Chrzan, A. Javey, *Adv. Mater.* **2016**, *28*, 4053.

[23] M. Velický, G. E. Donnelly, W. R. Hendren, S. McFarland, D. Scullion, W. J. DeBenedetti, G. C. Correa, Y. Han, A. J. Wain, M. A. Hines, D. A. Muller, K. S. Novoselov, H. D. Abruña, Robert M. Bowman, E. J. G. Santos, F. Huang, *ACS Nano* **2018**, *12*, 10463.

[24] Y. Huang, Y.-H. Pan, R. Yang, L.-H. Bao, L. Meng, H.-L. Luo, Y.-Q. Cai, G.-D. Liu, W.-J. Zhao, Z. Zhou, L.-M. Wu, Z.-L. Zhu, M. Huang, L.-W. Liu, L. Liu, P. Cheng, K.-H. Wu, S.-B. Tian, C.-Z. Gu, Y.-G. Shi, Y.-F. Guo, Z. G. Cheng, J.-P. Hu, L. Zhao, G.-H. Yang, E. Sutter, P. Sutter, Y.-L. Wang, W. Ji, X.-J. Zhou, et al., *Nat. Commun.* **2020**, *11*, 2453.

[25] J.-Y. Moon, M. Kim, S.-I. Kim, S. Xu, J.-H. Choi, D. Whang, K. Watanabe, T. Taniguchi, D. S. Park, J. Seo, S. Ho Cho, S.-K. Son, J.-H. Lee, *Sci. Adv.* **2020**, *6*, eabc6601.

[26] E. Pollmann, S. Sleziona, T. Foller, U. Hagemann, C. Gorynski, O. Petri, L. Madauß, L. Breuer, M. Schleberger, *ACS Omega* **2021**, *6*, 15929.

[27] F. Liu, W. Wu, Y. Bai, S. H. Chae, Q. Li, J. Wang, J. Hone, X.-Y. Zhu, *Science* **2020**, *367*, 903.

[28] M. Heyl, D. Burmeister, T. Schultz, S. Pallasch, G. Ligorio, N. Koch, E. J. W. List-Kratochvil, *Phys. Status Solidi RRL* **2020**, *14*, 2000408.

[29] S. E. Panasci, E. Schiliró, G. Greco, M. Cannas, F. M. Gelardi, S. Agnello, F. Roccaforte, F. Giannazzo, *ACS Appl. Mater. Interfaces* **2021**, *13*, 31248.

[30] H. M. Gramling, C. M. Towle, S. B. Desai, H. Sun, E. C. Lewis, V. D. Nguyen, J. W. Ager, D. Chrzan, E. M. Yeatman, A. Javey, H. Taylor, *ACS Appl. Electron. Mater.* **2019**, *1*, 407.

[31] S. Guo, D. Yang, S. Zhang, Q. Dong, B. Li, N. Tran, Z. Li, Y. Xiong, M. E. Zaghloul, *Adv. Funct. Mater.* **2019**, *29*, 1900138.

[32] Z. Li, L. Ren, S. Wang, X. Huang, Q. Li, Z. Lu, S. Ding, H. Deng, P. Chen, J. Lin, Y. Hu, L. Liao, Y. Liu, *ACS Nano* **2021**, *15*, 13839.

[33] H. Tabata, H. Matsuyama, T. Goto, O. Kubo, M. Katayama, *ACS Nano* **2021**, *15*, 2542.

[34] K. Novoselov, A. C. Neto, *Phys. Scr.* **2012**, *2012*, 014006.

[35] M. Velický, A. Rodriguez, M. Bousa, A. V. Krayev, M. Vondracek, J. Honolka, M. Ahmadi, G. E. Donnelly, F. Huang, H. D. Abruna, K. S. Novoselov, O. Frank, *J. Phys. Chem. Lett.* **2020**, *11*, 6112.

[36] C. Lee, H. Yan, L. E. Brus, T. F. Heinz, J. Hone, S. Ryu, *ACS Nano* **2010**, *4*, 2695.

[37] A. Rodriguez, M. Velický, M. Kalbáč, O. Frank, J. Řáhová, V. Zólyomi, J. Koltai, *Phys. Rev. B* **2022**, *105*, 195413.

[38] Z. Melnikova-Kominkova, K. Jurkova, V. Vales, K. Drogowska-Horná, O. Frank, M. Kalbac, *Phys. Chem. Chem. Phys.* **2019**, *21*, 25700.

[39] A. C. Ferrari, D. M. Basko, *Nat. Nanotechnol.* **2013**, *8*, 235.

[40] N. S. Mueller, S. Heeg, M. Peña-Alvarez, P. Kusch, S. Wasserroth, N. Clark, F. Schedin, J. Parthenios, K. Papagelis, C. Galiotis, M. Kalbac, A. Vijayaraghavan, U. Huebner, R. Gorbachev, O. Frank, S. Reich, *2D Mater.* **2018**, *5*, 015016.

[41] A. Das, S. Pisana, B. Chakraborty, S. Piscanec, S. K. Saha, U. V. Waghmare, K. S. Novoselov, H. R. Krishnamurthy, A. K. Geim, A. C. Ferrari, A. K. Sood, *Nat. Nanotechnol.* **2008**, *3*, 210.

[42] G. Froehlicher, S. Berciaud, *Phys. Rev. B* **2015**, *91*, 205413.

[43] Q. H. Wang, Z. Jin, K. K. Kim, A. J. Hilmer, G. L. Paulus, C.-J. Shih, M.-H. Ham, J. D. Sanchez-Yamagishi, K. Watanabe, T. Taniguchi, J. Kong, P. Jarillo-Herrero, M. S. Strano, *Nat. Chem.* **2012**, *4*, 724.

[44] C. Neumann, S. Reichardt, P. Venezuela, M. Drogeler, L. Banszerus, M. Schmitz, K. Watanabe, T. Taniguchi, F. Mauri, B. Beschoten, S. V. Rotkin, C. Stampfer, *Nat. Commun.* **2015**, *6*, 8429.

[45] T. Fan, A. A. Eftekhar, H. Taghinejad, P. Ajayan, A. Adibi, in *Laser Science*, Optica Publishing Group, Washington, D.C. **2016**, p. JTh2A–99.

[46] A. Rodriguez, M. Kalbáč, O. Frank, *2D Mater.* **2021**, *8*, 025028.

[47] R. Ganatra, Q. Zhang, *ACS Nano* **2014**, *8*, 4074.

[48] G. Haider, P. Roy, C.-W. Chiang, W.-C. Tan, Y.-R. Liou, H.-T. Chang, C.-T. Liang, W.-H. Shih, Y.-F. Chen, *Adv. Funct. Mater.* **2016**, *26*, 620.

[49] G. Haider, Y.-H. Wang, F. J. Sonia, C.-W. Chiang, O. Frank, J. Vejpravova, M. Kalbáč, Y.-F. Chen, *Adv. Opt. Mater.* **2020**, *8*, 2070075.

[50] B. K. Sarker, E. Cazalas, T.-F. Chung, I. Childres, I. Jovanovic, Y. P. Chen, *Nat. Nanotechnol.* **2017**, *12*, 668.

[51] C. Hu, X. Wang, B. Song, *Light: Sci. Appl.* **2020**, *9*, 88.

[52] Z. Ling, R. Yang, J. Chai, S. Wang, W. Leong, Y. Tong, D. Lei, Q. Zhou, X. Gong, D. Chi, K.-W. Ang, *Opt. Express* **2015**, *23*, 13580.